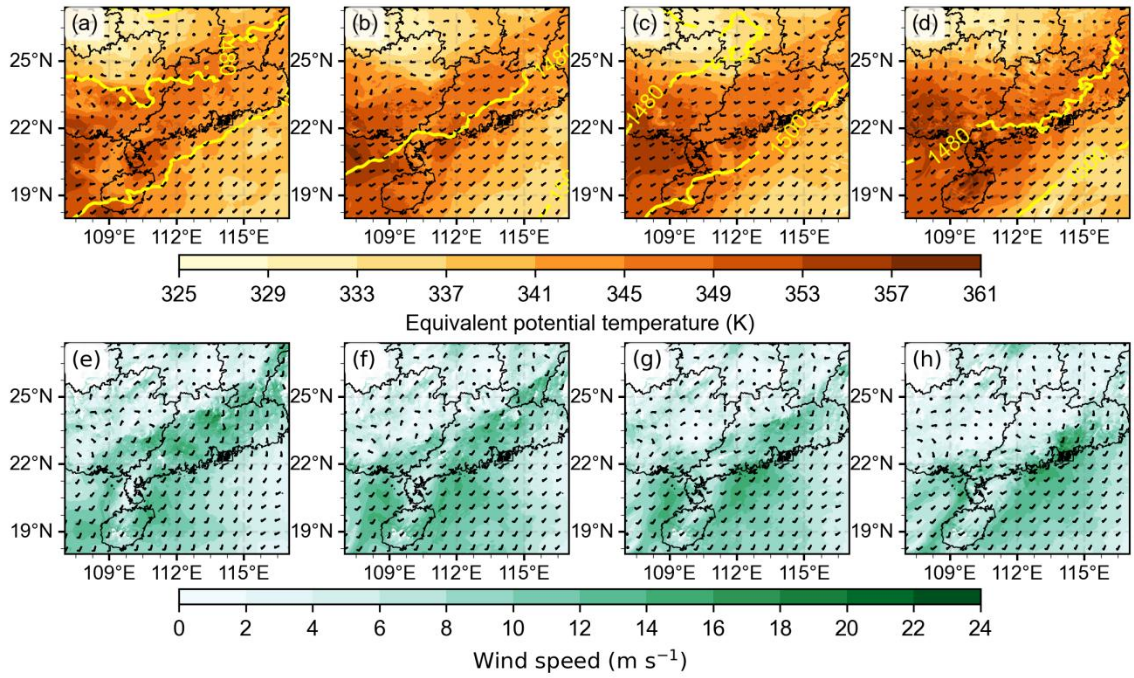

Fig. S1. Background fields in the d03 domain from 00:00 UTC 10 May to 12:00 UTC 11 May 2022. (a)–(d) 850-hPa pseudoequivalent potential temperature (shading; unit: K), geopotential height (yellow contours; unit: m), and wind field; (e)–(h) 925-hPa wind field (shading; unit: m s^{-1}).

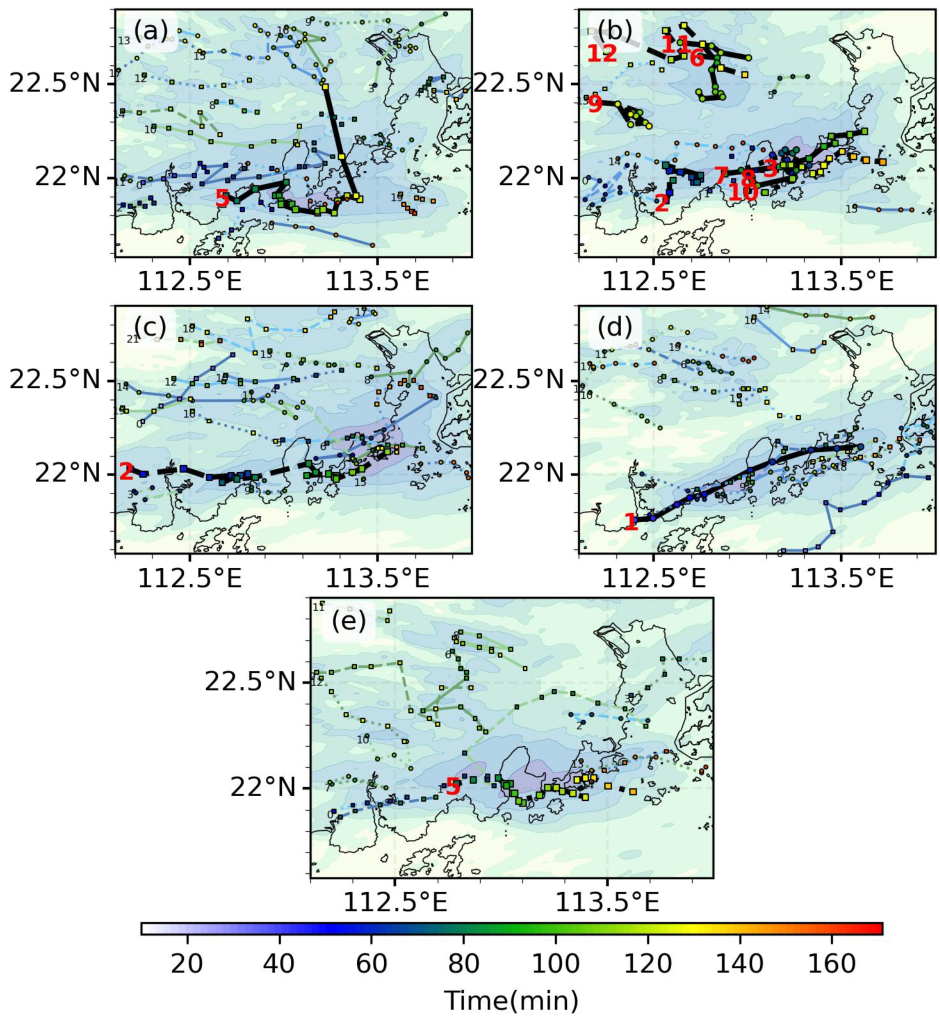

Fig. S2. Centroid movement tracks of intermediate-scale convective elements (MCEs) with lifetimes exceeding 1 h. Panels (a)–(e) correspond to the five experiments from MIN to MAX, respectively. Marker types and line colors/types distinguish different element tracks, and marker color denotes time since 18:00 UTC 10 May (unit: min).

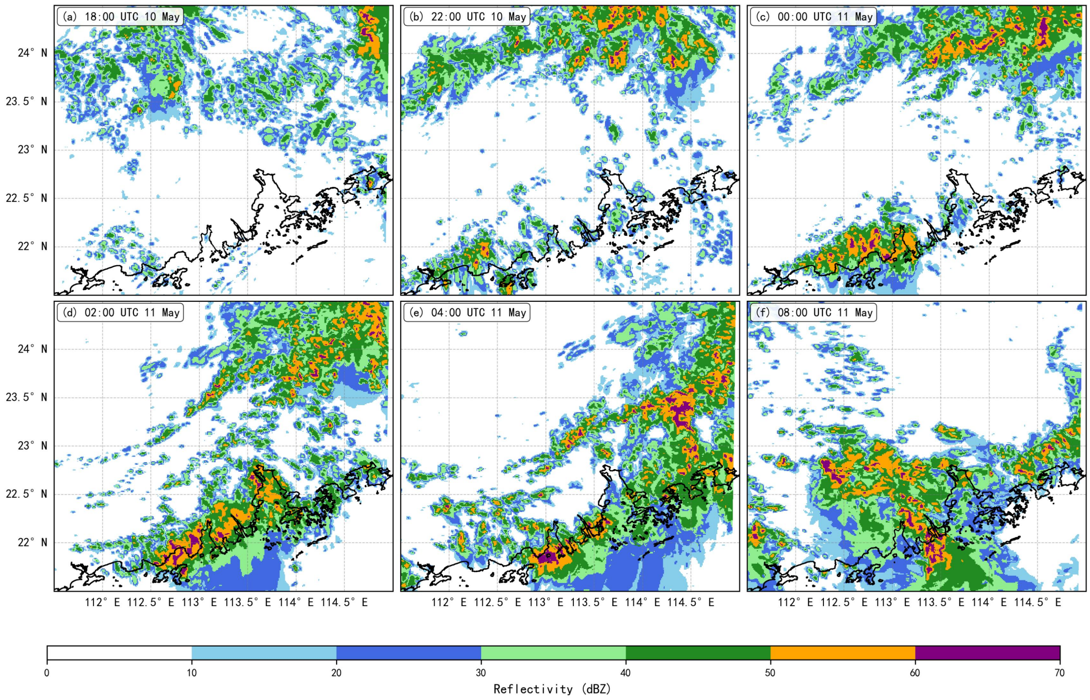

Fig. S3. Evolution of the spatial distribution of maximum composite radar reflectivity in the MIN experiment.

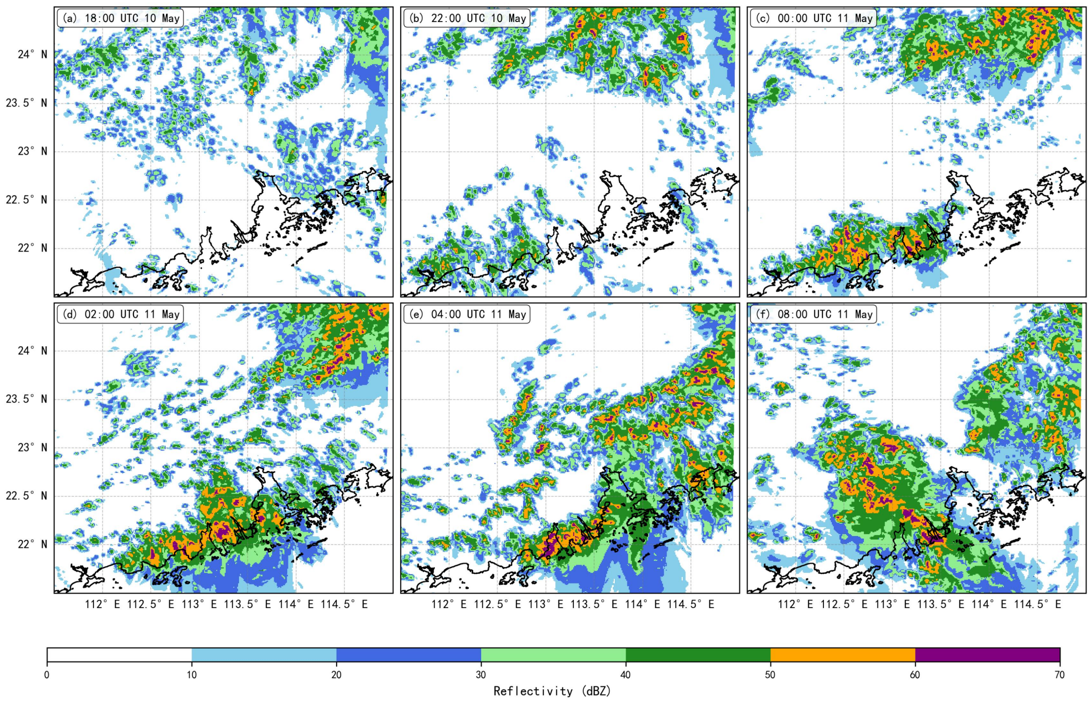

Fig. S4. Evolution of the spatial distribution of maximum composite radar reflectivity in the 025 experiment.

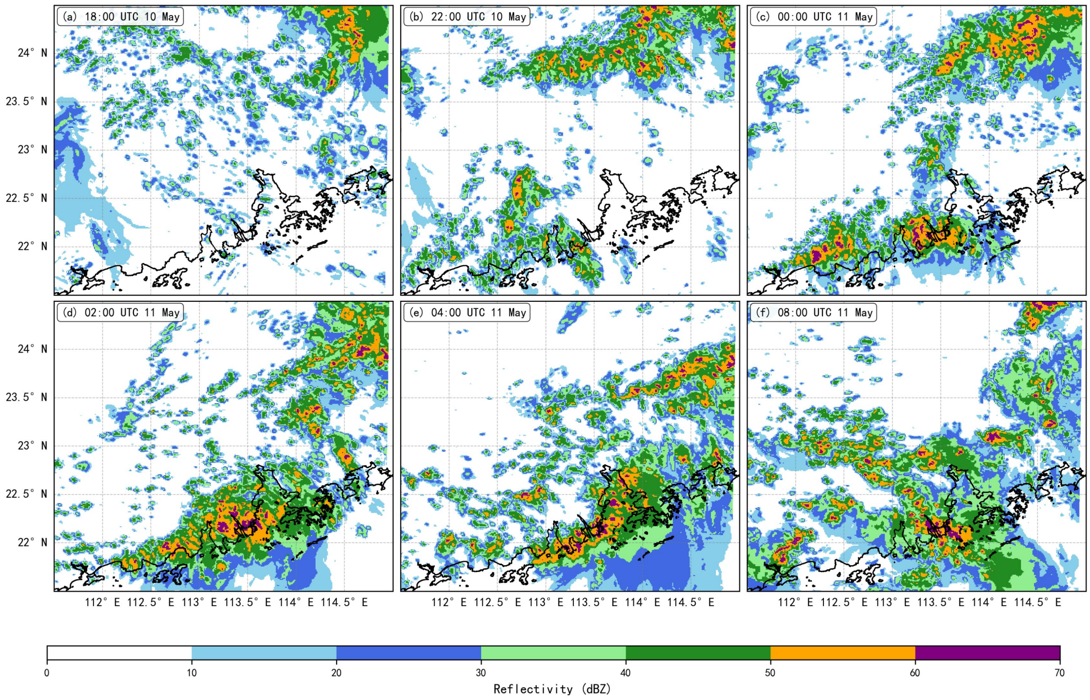

Fig. S5. Evolution of the spatial distribution of maximum composite radar reflectivity in the AVE experiment.

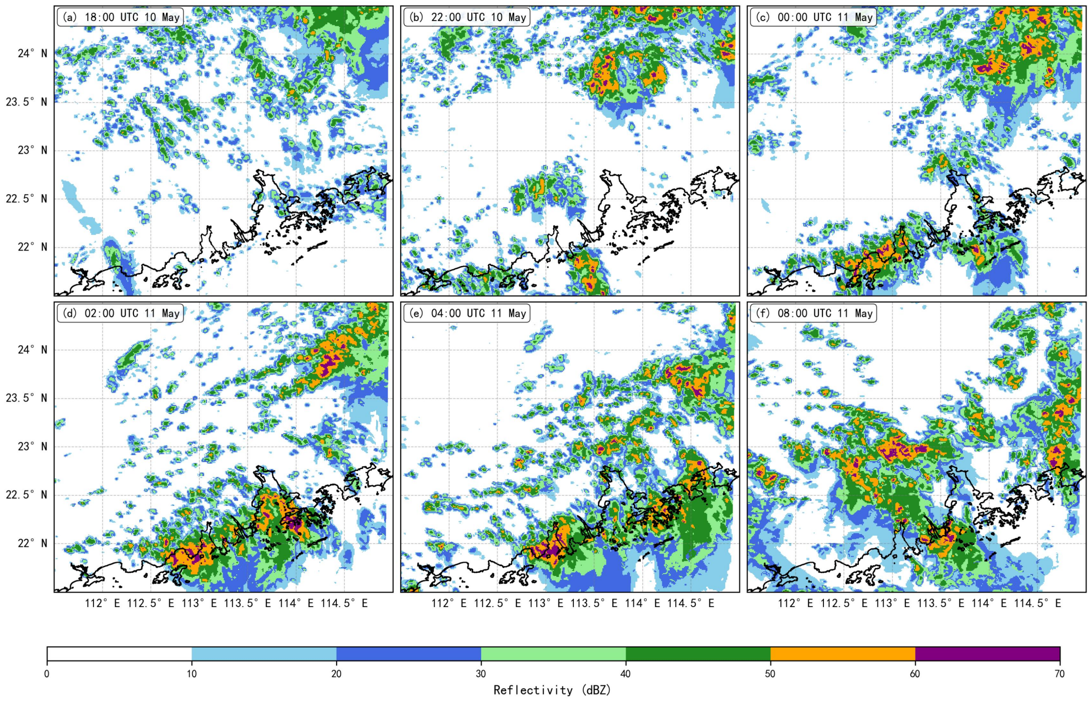

Fig. S6. Evolution of the spatial distribution of maximum composite radar reflectivity in the 075 experiment.

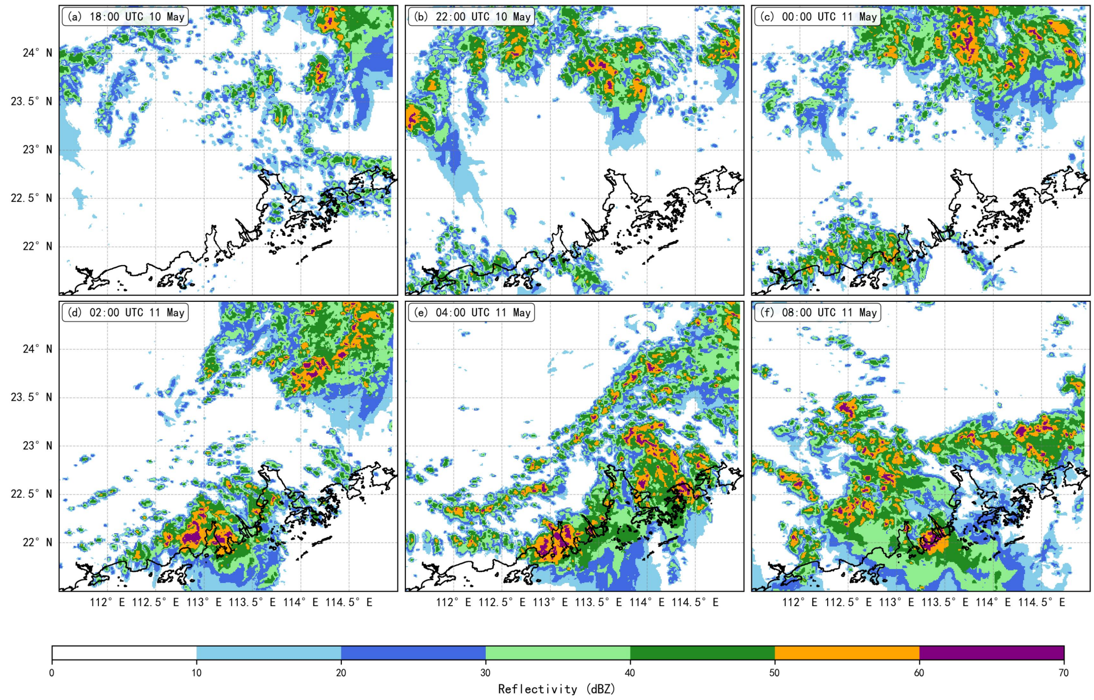

Fig. S7. Evolution of the spatial distribution of maximum composite radar reflectivity in the MAX experiment.

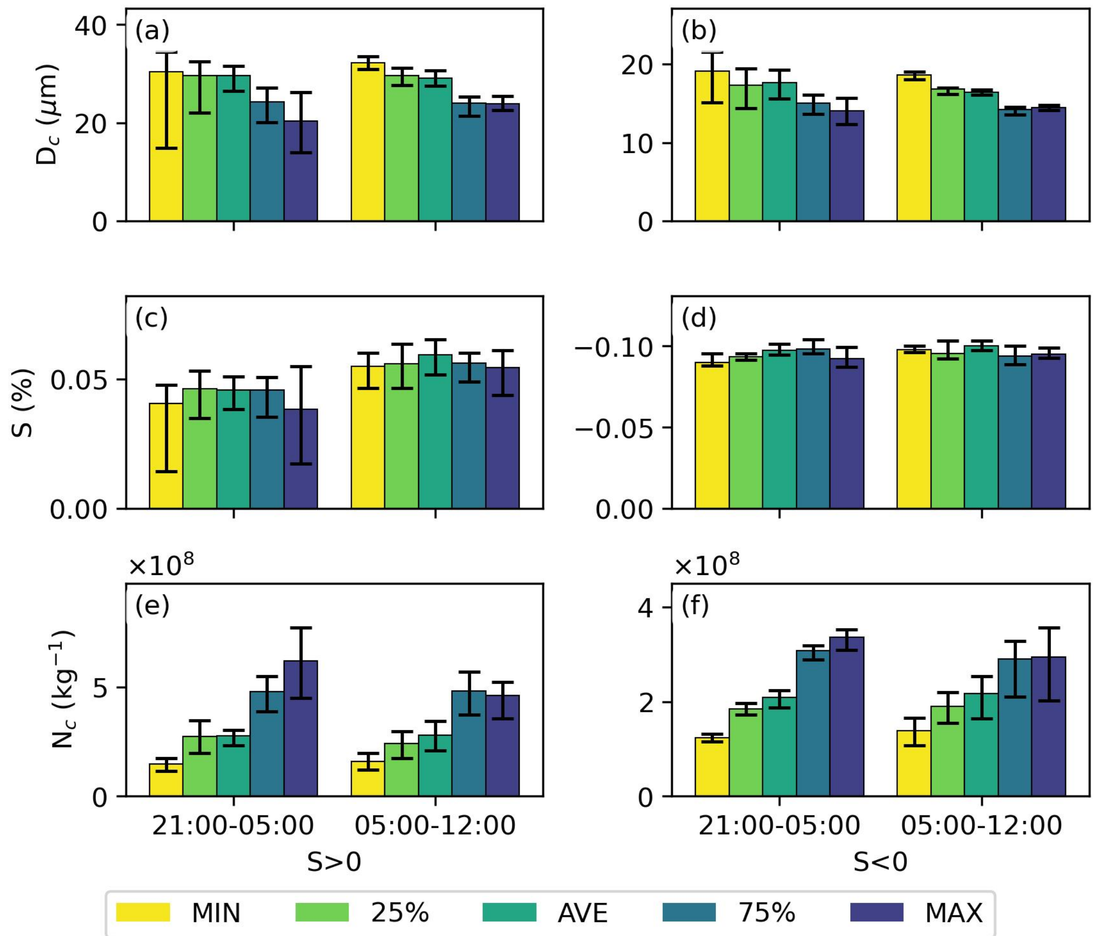

Fig. S8. Cloud-microphysical statistics in condensation regions (S > 0) and evaporation regions (S < 0) under different aerosol backgrounds. (a, b) Mean cloud-droplet diameter (unit: μm); (c, d) relative supersaturation; (e, f) cloud-droplet number concentration (unit: m^{-3}). Bar height represents the regional mean, and error bars span the 20th–80th percentile range.

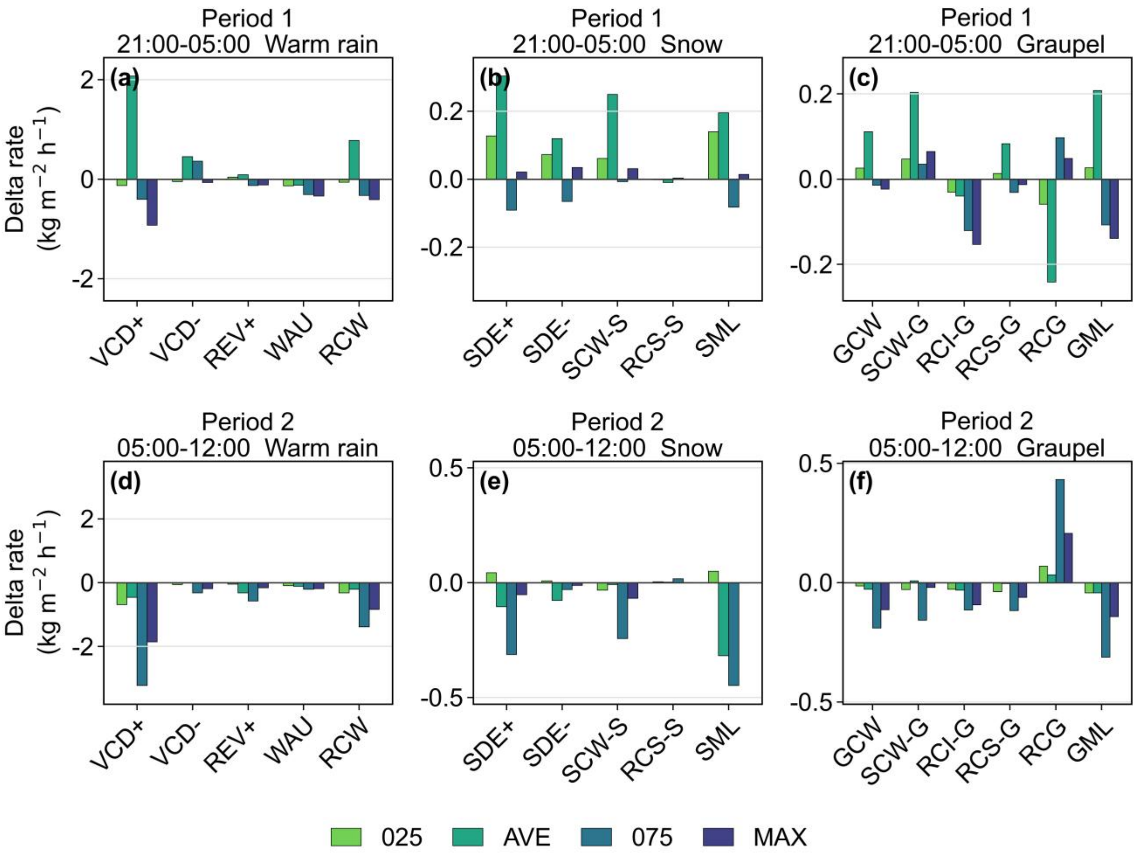

Fig. S9. Differences in study-area-mean microphysical process conversion rates relative to MIN. (a–c) Warm-rain-, snow-, and graupel-related processes during the primary-rainband development stage; (d–f) corresponding processes during the later organizational adjustment stage. VCD, REV, WAU, and RCW denote cloud-water condensation/evaporation, raindrop evaporation/condensation, autoconversion of cloud water to rainwater, and collection of cloud water by raindrops, respectively; SDE, SCW-S, RCS-S, and SML denote snow deposition/sublimation, collection of supercooled cloud water by snow, collection of snow by raindrops, and snow melting; GCW, SCW-G, RCI-G, RCS-G, RCG, and GML denote collection of cloud water by graupel, production of graupel by snow collecting supercooled cloud water, production of graupel by raindrops collecting ice crystals, production of graupel by raindrops collecting snow, collection of graupel by raindrops, and graupel melting. "+" and "–" denote the positive and negative branches of each process, respectively. Unit: kg m^{-2} h^{-1}.

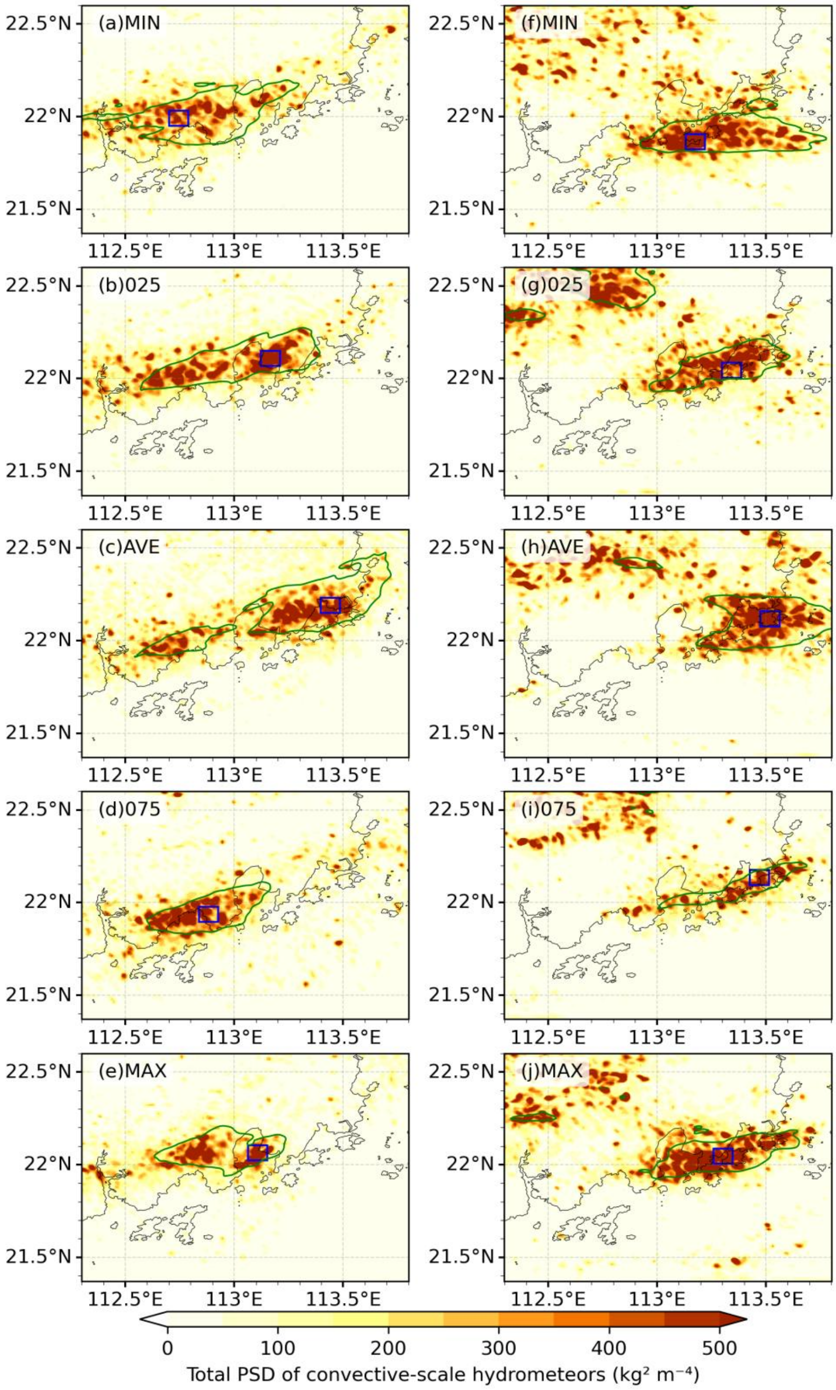

Fig. S10. Spatial distribution of total convective-scale hydrometeor power spectral density (shading; unit: kg² m⁻⁴) and selected convective-core areas for each experiment during the primary-rainband development stage (a–e) and later organizational adjustment stage (f–j). The green contour denotes 100 mm accumulated precipitation for the corresponding stage.

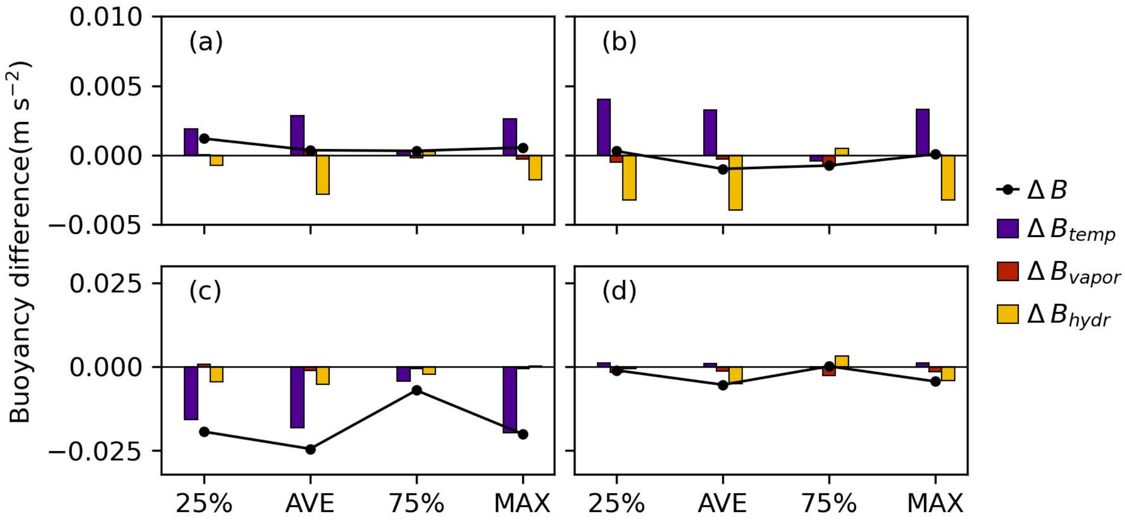

Fig. S11. Differences in the vertical distributions of buoyancy components at the convective scale relative to MIN. (a) and (b) correspond to the primary-rainband development stage and later organizational adjustment stage below 5 km; (c) and (d) correspond to the same two stages above 5 km. Unit: m s^{-2}.